Extratropical circulation associated with Mediterranean droughts during the Last Millennium in CMIP5 simulations

Woon Mi Kim[1,2,3], Santos J. González-Rojí[1,2], and Christoph C. Raible[1,2]

[1]Climate and Environmental Physics, University of Bern, Bern, Switzerland
[2]Oeschger Centre for Climate Change Research, University of Bern, Bern, Switzerland
[3]Now at: National Center for Atmospheric Research, Boulder Colorado, United States

Correspondence: Woon Mi Kim (wmikim@ucar.edu)

Abstract.

Knowing that internal climate variability is the principal driver of Mediterranean droughts during the last millennium, in this study, we investigate circulation patterns in the Euro-Atlantic domain associated with multi-year droughts over the Mediterranean region in CMIP5-PMIP3 and CESM-LME simulations. The focus is on the natural variability of droughts during

5   850–2005, thus excluding the anthropogenic trends from 1850 CE onward. The results re-confirm that Mediterranean drought occurrence during the last millennium is associated with internal variability. In terms of the temporal variability, all climate models exhibit a multi-decadal anti-phase occurrence of droughts between the western and eastern Mediterranean agreeing with some proxy records. This anti-phase occurrence of droughts can be explained by the dominant circulation patterns in each region: western Mediterranean droughts are dominated by a high-pressure system and ridge over central Europe and an

10 NAO-like pattern, while eastern Mediterranean droughts are linked to positive pressure anomalies in the southern and eastern Mediterranean, negative NAO, negative EA and EA-WR-like patterns. However, these modes of climate variability are strongly model-dependent, i.e. each model has its preferred circulation patterns that occur more frequently during droughts, suggesting that the main drivers of droughts differ between the models. The models' preference is therefore a potential source of uncertainties in Mediterranean droughts in model-proxy comparison and may have implications for future climate projections.

1   Introduction

Droughts are recurrent climate events in the Mediterranean region where precipitation shows a high spatial and interannual variability (Lionello et al., 2006). The complex spatial and temporal characteristics of Mediterranean precipitation and hydroclimate are due to its geographical location, extending latitudinally from the semi-arid subtropics to temperate mid-latitudes, and strong seasonal influences of the subtropical high in the Atlantic Ocean, teleconnections, and large-scale modes of variabil-

20 ity (Rodwell and Hoskins, 1996; Krichak and Alpert, 2005; Lionello et al., 2006). The climate of the Mediterranean region is characterized by a wet winter and hot dry summer, receiving a large proportion of precipitation originated from the mid-latitude circulations and westerlies during the winter (Lionello et al., 2006). Hence, winter is the crucial season for moisture supply that determines the intensity of drought impacts on the region.

Although droughts are natural fluctuations of this region with highly variable seasonal hydroclimate conditions, future cli-
25   mate projections indicate robust increases in drought frequencies and intensities over the Mediterranean region even under
stricter mitigation scenarios (Lehner et al., 2017; Samaniego et al., 2018; Masson-Delmotte et al., 2021). This change is prin-
cipally attributed to the intensification of the global hydrological cycle caused by anthropogenic influences in the atmosphere
(Masson-Delmotte et al., 2021). In the Mediterranean region, precipitation is expected to decrease due to an expanding Hadley
Cell (Previdi and Liepert, 2007) and a poleward shift of the mid-latitude storm tracks (Yin, 2005; Wu et al., 2011). The most sig-
30   nificant change will occur in the winter precipitation and its associated circulation, which is partially contributed by a decrease
in the regional land-sea temperature gradient (Tuel and Eltahir, 2020). In addition to that, the future increase in temperature
will amplify land-atmosphere feedbacks and vapour pressure deficit, which will potentially enhance the intensity of droughts
(Zhou et al., 2019).

Up to date, circulations associated with future potential changes in hydroclimate including persistent droughts are extensively
35   studied in the region (e.g., Dubrovský et al., 2014; Spinoni et al., 2020; Tramblay et al., 2020; Cos et al., 2022). However, how
drought-associated circulations look like before the anthropogenic greenhouse gas (GHG) era is comparably less explored.
Long past climate data enable us to examine persistent droughts, which are the conditions that can possibly be comparable to
the future drying over the region, and their long-term variability that cannot be captured in the limited-length observational-
based records. Among the past periods, the last millennium is of particular interest as it is a relatively close time period with no
40   strong change in climate boundary conditions and with abundant high-quality proxy-based reconstructions (PAGES Hydro2k
Consortium et al., 2017).

Several natural proxy-based reconstructions of past hydroclimate have contributed to a better understanding of droughts
variability and their associated climate modes during the last millennium (PAGES Hydro2k Consortium et al., 2017). One
of the widely used proxy-based datasets is a tree ring-based reconstruction of summer dry and wetness in Europe, known
45   as the Old World Drought Atlas (OWDA; Cook et al., 2015). Using OWDA, Cook et al. (2016) identified a multi-decadal
in-phase drought occurrence across the Mediterranean basin and an anti-phase occurrence within the eastern Mediterranean.
This result contradicts the finding by Roberts et al. (2012) based on the lake sediment records, which have shown an anti-phase
hydroclimate variability between the western and eastern Mediterranean from the Medieval Climate Anomaly period. Different
proxy-based studies have indicated that the Mediterranean hydroclimate's variability is influenced by several modes of climate
50   variability and atmospheric circulation, such as Eastern Atlantic Pattern (EA; Cook et al., 2015), and North Atlantic Oscillation
(NAO; Cook et al., 2015; Baek et al., 2017; Markonis et al., 2018). In a long-term analysis for the entire last millennium,
Markonis et al. (2018) found that over southern Europe including the Mediterranean, drier conditions have become dominant
in the 20th century exceeding the millennial hydroclimate boundaries. Regarding natural external forcing, volcanic eruptions
that are the natural radiative forcing with the strongest impact on the global climate during the last millennium, have caused
55   wetter conditions that last up to a few years after the first emissions (Gao and Gao, 2017; Rao et al., 2017).

Besides proxy-based reconstructions, climate models have been useful tools to support findings from proxy-based studies.
Since climate simulations can cover the temporal resolutions and time periods that go beyond the time scales of proxy records,
they can provide more insight into the variability and mechanisms of past hydroclimate and droughts. For instance, the impact

of volcanic eruptions on long-lasting droughts was assessed on a global scale (Stevenson et al., 2017) and the Mediterranean
60   region (Kim and Raible, 2021) using the Community Earth System Model (CESM; Lehner et al., 2015; Otto-Bliesner et al.,
2016). With the same model, Kim and Raible (2021) found that persistent Mediterranean droughts in the last millennium
are associated with modes of internal climate variability, with a strong influence of positive NAO and higher than normal
regional temperatures. Other studies come to the same conclusion, e.g., Xoplaki et al. (2018) showed that changes in the
eastern Mediterranean hydroclimate are explained by internal variability in CCSM4 and MPI-ESM simulations. They also
65   found that the type of internal variability is model-dependent.

Despite these past studies on the Mediterranean hydroclimate, circulation patterns associated with multi-year persistent
droughts during the last millennium are still not fully explored in currently available climate simulations. If internal variability
is an important driver of droughts before the pre-industrial period, it is necessary to understand which modes of climate
variability or circulation patterns are involved in each climate model, and whether these patterns are depicted in the same
70   way in all model simulations. The focus of this study is on the patterns in the mid-latitudes that have more impacts on the
Mediterranean hydroclimate.

In this study, we examine extratropical circulation patterns in the Euro-Atlantic domain associated with the western (12°W–
19°E, 32°–43°N) and eastern (19°–37°E, 32°–43°N) Mediterranean droughts during the last millennium (850–2005) using
the model simulations from the fifth phase of the Climate Model Intercomparison Project (CMIP5; Taylor et al., 2012) -
75   Paleoclimate Model Intercomparison Project Phase 3 (PMIP3; Schmidt et al., 2012) and CESM Last Millennium Ensemble
Project (CESM-LME; Otto-Bliesner et al., 2016). All the details of the datasets are provided in Section 2. Soil moisture
anomalies are employed as a drought metric in this study, and commonly used statistical techniques in climate sciences are
applied to detect circulation patterns. The information about these methods is presented in Section 3. Drought periods and main
circulation patterns are identified in the climate model simulations and compared to each other in Section 4. This study ends
80   with a discussion of the results in Section 5, followed by the concluding remarks in Section 6.

2   Data

2.1   CMIP5-PMIP3 model simulations

To study drought variability and the associated extratropical circulation patterns during 850–2005, we use several transient
simulations of Last Millennium (LM; 850–1850) and historical period (Hist; 1850–2005) from the CMIP5-PMIP3 and CESM-
85   LME projects. We consider only simulations that provide the vertical water content of each soil layer (variable names *mrlsl*
in PMIP3-CMIP5, and *SOILLIQ* and *SOILICE* in CESM-LME). Thus, only four climate model simulations are used for the
analysis: GISS-E2-R, CCSM4, bcc-csm1-1, and MIROC-ESM. For CESM-LME we use 12 ensemble members of CESM1.
The vertical water content of soil layers is employed to quantify soil moisture droughts. Surface temperature and geopotential
height at 500 hPa are retrieved to describe the mean temperature and circulation conditions during Mediterranean drought
90   years. All variables have a monthly temporal resolution, but different horizontal and vertical land resolutions as shown in
Table 1. Additional specifications of each model are summarized there. All simulations were run with the volcanic, solar, and

greenhouse gas (GHG) forcings agreed upon by the PMIP3-CMIP5 protocol (Schmidt et al., 2012; Taylor et al., 2012). For GISS-E2-R in the LM experiment, three realizations (*i1r1p122*, *i1r1p125*, and *i1r1p128*) that were run with the same volcanic forcing are considered in the analysis.

Table 1. Details of the climate models and simulations used for the analysis. LM and Hist indicate the last millennium and historical experiments, respectively.

Model	Number of Ensemble Members		Horizontal resolution	Vertical soil layers up to 70 cm	Number of grid points	
	LM	Hist			West	East
CESM1	12	12	$1.875° \times 2.5°$	7	85	46
GISS-E2-R	3	3	$2° \times 2.5°$	7	85	46
CCSM4	1	3	$1° \times 1.25°$	7	173	99
bcc-csm1-1	1	3	$2.8° \times 2.8°$	7	38	25
MIROC-ESM	1	3	$2.8° \times 2.8°$	3	22	12

2.2 Observation-based data

Since observations of subsurface soil moisture content are spatially scarce, we use soil moisture content from the Noah land surface model (NOAH-LSM), which is a part of the Global Land Data Assimilation System 2.1 (GLDAS2.1; Rodell et al., 2004). NOAH-LSM is a physical land model that solves and quantifies the transfer of heat and moisture at the surface to the subsurface levels and interactions between the soil, atmosphere and vegetation. The model is forced by atmospheric conditions from satellite- and ground-based observational data products. The soil moisture variable from NOAH-LSM has four layers up to two meters, with monthly temporal and $1°$ spatial resolutions extending from 1948 to the present.

To characterize the atmospheric circulation we use the monthly mean geopotential height at 500 hPa from the ERA5 reanalysis (Hersbach et al., 2018, 2020). ERA5 is the latest reanalysis product of the European Centre for Medium-Range Weather Forecasts (ECMWF), and the products are generated with the 2016 version of the ECMWF numerical weather prediction model and the integrated forecasting system Cy41r2 data assimilation. The spatial resolution of ERA5 is $0.25°$ and the temporal extent is from 1950 to the present. For the analysis, ERA5 data is horizontally interpolated to $1°$ spatial resolution to match the resolution of NOAH-LSM.

3 Methods

3.1 Calculation of anomalies

110 The following variables from the NOAH-LSM, ERA5, and climate simulations are used in the analysis: the surface temperature, geopotential height at 500 hPa, and soil moisture content at vertical soil layers. These variables are transformed into the annual mean anomalies at each grid point. We use annual mean anomalies in order to include winter conditions in the analysis, as it is an important season for the annual hydroclimate in the Mediterranean. Prior to the anomaly calculation, the soil moisture content of soil layers from NOAH-LSM and climate models are vertically integrated to 70 cm. If the exact 70 cm level is not

115 available, the vertically integrated soil moisture is linearly interpolated over depth to the 70 cm level.

Then, first, the monthly anomalies are calculated by subtracting the multi-year monthly means from each of the monthly values. Different reference periods for the multi-year monthly means are used depending on the periods of study and experiments. For the observational-based data, NOAH-LSM and ERA5, the reference period is 1950–1979. For the LM and Hist experiments in the climate models, the period 850–1849 is used. Second, the necessary annual mean anomalies are obtained

120 by averaging annually these monthly anomalies.

In addition, we remove the strong unprecedented trends in the Hist simulations (1850–2005). Thereby, the ensemble means of the anomalies are calculated and subtracted from each of the ensemble member anomalies at each grid point employing a similar method to Maher et al. (2018). This method guarantees that only internally driven variability remains in the time series of the variables. This method is not applied to the LM period, therefore, the LM anomalies still contain forced signals such as

125 those from volcanic eruptions. Note that the number of ensemble members can have an influence on the final output of Hist. The potential implications of this method are discussed in Section 5.

The two periods, LM and Hist, are merged into one time series, and droughts are estimated for each of the models and regions. The number of drought years is counted with a moving window of a century, and a percentage of total drought years (years with droughts in all ensemble members divided by the total model years) and a mean duration of droughts are calculated

130 for each of the models and regions.

3.2 Region of study

Similar to Cook et al. (2016), we separate the Mediterranean into two subregions: the western Mediterranean encompassing 13°W–19°E, 32°–43°N and the eastern Mediterranean occupying 19°–37°E, 32°–43°N. The separation is motivated by the suggested influences of the circulation patterns over the Mediterranean region (Dünkeloh and Jacobeit, 2003; Lionello et al.,

135 2006), such as the NAO, EA, Eastern Atlantic-West Russian (EA-WR), and the Scandinavian patterns. The western Mediterranean is more intensely influenced by NAO than the eastern region, and the eastern region is not only affected by NAO but also strongly linked with East Atlantic-type patterns.

3.3 Comparison between present-day observation-based data and model simulations

Pearson correlation coefficients (PCC) are calculated between the annual soil moisture anomalies (SOIL) of the western and
140 eastern Mediterranean, and the geopotential height anomalies (Z500) in the north Atlantic and European domain (70°W–70°E,
21°–85°N). SOIL is from NOAH-LSM and Z500 from ERA5, both obtained from Section 3.1. The PCC allows us to measure
the link between the soil moisture variability and circulations in the present day. The period for the correlation is 56 years from
1950 to 2005. Assuming that NOAH-LSM represents realistically soil moisture variability, the correlation patterns of other
climate models are compared against the pattern of NOAH-LSM.

145 3.4 Drought definition

The annual anomalies of vertically integrated soil moisture at 70 cm (SOIL) in LM and Hist are used as the metric to quan-
tify annual droughts. The 70 cm level is a deep soil level that can reflect the impacts of soil moisture change on vegetation
and ecosystems, hence, better-representing soil moisture droughts including their persistent characteristics (Dirmeyer, 2011;
Ghannam et al., 2016; Esit et al., 2021).

150 Two temporal and spatial criteria are applied to detect droughts over each of the study regions:

   i) We combine two definitions used by Kim and Raible (2021) and Coats et al. (2013): a drought must be composed only
   of negative SOIL (Kim and Raible, 2021), and it must commence after two consecutive years of negative SOIL and
   continue until two consecutive years of positive anomalies (Coats et al., 2013). Thereby, we ensure that droughts are
   intense enough as they are composed of only negative values without being interrupted by a particularly wet year in
155   between. This definition also assures a minimum drought duration of two years. Using these definitions, droughts are
   detected at each horizontal grid point in the study regions.

   ii) A spatial restriction is applied to the detected drought years to be considered as a regional-scale drought (western or
   eastern). At least 60% of the horizontal grid points over the region (the western or eastern Mediterranean) need to be
   under negative SOIL conditions during all consecutive drought years. This guarantees that droughts are regional and not
160   local events.

When these temporal and spatial criteria are fulfilled, droughts are identified for all grid cells. At this step, we do not
apply any horizontal interpolation in SOIL. Thus, regional coverage (geographical extension and number of grid cells) differs
slightly between the models (as shown in Table 1). Nevertheless, this approach avoids changes in the initial SOIL values, as
hydroclimate variables associated with precipitation can be sensitive to the horizontal grid resolution (Champion et al., 2011;
165 Kopparla et al., 2013; Haren et al., 2015). Also, in this way, the effects of the number of land grid cells on drought estimation
and drought-associated circulation can be identified. Next, the weighted spatial average of SOIL is calculated to generate a
time series for the western and eastern Mediterranean.

Finally, a drought is considered regional (only west- or east-occurring) when the temporal overlap during one drought event
between the two regions is less than 50%. When the temporal overlap is more than 50%, the event is considered a pan-

Mediterranean drought. The analysis focuses on only west and east-occurring droughts. The reason is that pan-Mediterranean droughts are rather rare events. Only climate models with some ensemble members in LM, such as CESM1 and GISS-E2-R, show few numbers of pan-Mediterranean droughts. Other models only present one or two drought events with Pan-Mediterranean characteristics. In the Hist simulations, when the anthropogenic signals are removed (Section 3.1), pan-Mediterranean droughts are not detectable.

3.5 Extratropical circulation pattern detection: principal component, k-mean clustering and Pearson correlation analyses

Drought-associated circulation patterns are detected in the model simulations using Z500 over 70°W–70°E, 21°–85°N during drought years. All Z500 fields are interpolated to a common horizontal resolution of CESM1 (Table 1).

The method for pattern detection consists of a combination of standard statistical methods in climate sciences: a principal component (PCA), k-mean clustering (KCA), and Pearson correlation analysis (PC-KCA-PCC method). The flow chart in Fig. 1 illustrates all the steps from the definition of drought (step 1, Section 3.4) to the detection of associated circulation patterns.
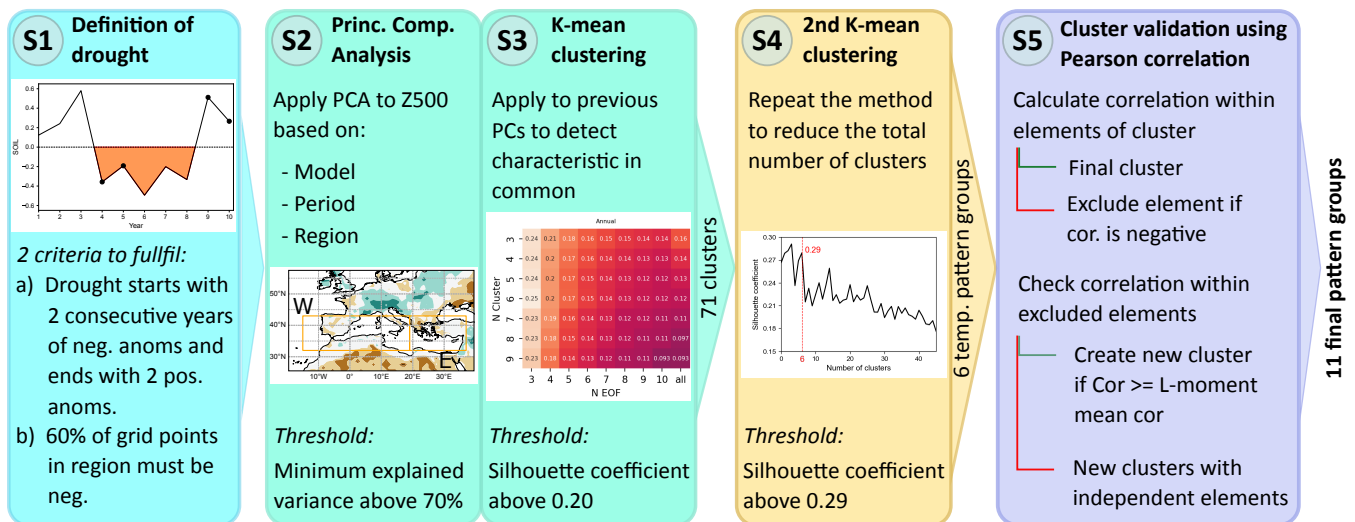
Figure 1. Flow chart summarizing the procedure for the detection of the extratropical circulation patterns associated with the Mediterranean droughts. The diagram includes the following steps: the definition of drought, the principal component analysis, the K-mean clustering, and the Pearson correlation analysis. A detailed description of each step can be found in Sections 3.4 and 3.5.

After obtaining drought years in step 1, in step 2 the PCA technique is applied to the Z500 fields. PCA allows a decomposition of a spatio-temporal field $X(t,s)$ into spatial patterns $u_k(s)$ (s being the spatial dimensions) and its associated temporal indices $T_k(t)$ (t the time steps, here years) for a number of modes M contained in the field (Hannachi et al., 2007). PCA is

based on the following equation:

$$X(t,s) = \sum_{k=1}^{M} T_k(t) \cdot u_k(s) \tag{1}$$

PCA provides a new set of uncorrelated linear combinations of the original field (principal components; PC) that captures its original variance. Each PC has an associated decreasing explained variance. By truncating the number of PCs according to a certain threshold, PCA can serve as a tool to filter the original data by reducing the dimension of multi-dimensional dataset (Monahan et al., 2009). In this study, PCA is applied to the Z500 fields during droughts for each model, experiment — LM or Hist —, and region — the western or eastern Mediterranean. The minimum threshold considered for the truncation of PCs is 70%. The truncation reduces substantially the number of retained PCs N and increases the performance of KCA in the next step.

In step 3, KCA is applied to the fields of PCs to detect the characteristic circulation patterns during droughts. KCA is an unsupervised classification technique that aims to cluster variables by their similarities minimizing the distance between the data points x_i and between the potential clusters c_k (Wilks, 2011; Zscheischler et al., 2012). Hence, it attempts to minimize the clustering objective function Q by

$$Q(c_1, ..., c_k) = \frac{1}{n} \sum_{i=1}^{n} min_{k=1,...,k} \|x_i - c_k\|^2 \tag{2}$$

where k is the number of clusters and n is the number of data points. KCA has the advantage of repeating the calculation in equation 2 until the best set of k number of clusters is found. The number of PCs N and clusters k is not determined in the beginning. We calculate the mean Silhouette coefficients S (Shahapure and Nicholas, 2020) for a range of N and k to find the optimal N and k (step 3 in Fig. 1). A mean Silhouette coefficient S is a metric that measures the quality of clustering by considering the similarity within the same cluster and the dissimilarity between the clusters. To get the mean Silhouette coefficient S, a Silhouette coefficient s for each data point is first calculated by

$$s = \frac{b - a}{max(a,b)} \tag{3}$$

where a is the mean distance within the same cluster, and b is the mean distance to the nearest neighbouring cluster. All the s for each point are averaged to obtain S. S ranges between -1 and 1, 1 indicating an optimum cluster showing a high similarity between its elements and a high distance to the neighbouring clusters. Then, the N and k with the highest S are selected. Through this PC-KCA process, 71 clusters are obtained, which characterize Z500 during droughts for each model, period and region. The variance explained by the PCs, the number of clusters and the mean Silhouette coefficients obtained during the PC-KCA steps can be found in Table 2. The supplement to this paper includes the full range of silhouette coefficients obtained for each model and period (LM and Hist simulations in Fig. S1 and Fig. S2, respectively).

In step 4, these 71 clusters (from now on, *cluster*) are re-clustered through KCA and Pearson correlation analysis in order to gather similar clusters between all the models, periods, and regions (steps 4 and 5 in Fig. 1, respectively). After that, we will define the final groups of drought-associated circulation patterns (from now on, *pattern group*). For this, first, KCA is applied

Table 2. Percentages of variance explained by N number of principal components (PC), k number of clusters, and mean Silhouette coefficients S obtained by the PC-KCA steps of the pattern detection according to the model, Mediterranean region and period considered.

Model	Region	Last Millennium (LM)			Historical (Hist)		
		% Variance (N PC)	k Clusters	S Coefficient	% Variance (N PC)	k Clusters	S Coefficient
CESM1	West	77.91 (5)	3	0.17	79.82 (5)	3	0.23
	East	78.60 (5)	3	0.18	79.82 (5)	3	0.20
GISS-E2-R	West	75.11 (5)	3	0.19	75.78 (5)	7	0.22
	East	73.63 (6)	3	0.17	77.60 (5)	3	0.22
CCSM4	West	77.03 (5)	4	0.18	80.20 (5)	3	0.18
	East	74.43 (5)	3	0.19	80.56 (5)	3	0.24
bcc-csm1-1	West	77.01 (5)	3	0.19	83.93 (5)	3	0.26
	East	75.34 (5)	6	0.19	80.95 (5)	3	0.23
MIROC-ESM	West	72.90 (5)	5	0.18	76.05 (5)	3	0.24
	East	75.13 (6)	3	0.17	79.85 (5)	4	0.19
Total 71 clusters							

to the 71 clusters to get the temporary pattern groups. $k = 6$ is used as the mean Silhouette coefficient S decreases abruptly (step 4 in Fig. 1).

The final step 5 assures the similarity between the clusters within the same pattern group (step 5 in Fig. 1). For this, we
220   calculate the Pearson correlation coefficients r (PCC; Wilks, 2011) between the clusters of the same pattern groups. Within the same pattern group, if one cluster is negatively correlated with one or more cluster members, this cluster is excluded from the pattern group. The mean r of the pattern group is again calculated without the excluded clusters. Next, r is calculated between each excluded cluster and members of the other pattern groups to determine if the excluded cluster can join a new pattern group. The criteria to join the pattern group is that the excluded cluster must show a positive r with all cluster members of
225   the target pattern group, and the r must be more than the minimum mean r among the existing pattern group. This process is repeated to all excluded clusters from the six temporary pattern groups. If this reorganization of clusters is not successful for some excluded clusters, r is calculated between those clusters which are not assigned to any of the existing pattern groups. When some remaining clusters are positively correlated with each other with a mean r of more than the minimum mean r among the existing pattern group, they are gathered to create a new pattern group. This re-assignment is repeated until no more
230   gathering is possible. This thorough process leaves 11 pattern groups that represent the circulation patterns associated with drought conditions in the Mediterranean region.

4 Results

4.1 Observation-model comparison (1950–2005)

Fig. 2 shows SOIL from NOAH-LSM and the mean SOIL of five climate models with the ensemble spread. SOIL from NOAH-
235 LSM is within the range of the CMIP5-PMIP3 model ensemble spread except for one year in 1975. The unprecedented trends
in SOIL are clearly visible in the models from 1850 onward (Fig. 2b and c). As described in Section 3.1, these trends were
removed by subtracting from each of the ensemble members the anomalies at each grid point.

The spatial correlations between SOIL and Z500 of NOAH-LSM and each of the climate simulations are presented in
Fig. 3. In all simulations, SOIL is negatively correlated with Z500 in the western (Fig. 3a) or eastern Mediterranean (Fig. 3b).
240 This indicates that a decrease in SOIL is associated with a high Z500, which is a typical atmospheric circulation during dry
conditions. A high-pressure system and a ridge over a region are associated with stable atmospheric conditions with a clear
sky and high temperature, which can induce an initial increase in evapotranspiration that accelerates a loss of soil moisture.
In addition, the anticyclonic circulation hampers incoming moisture fluxes from the Atlantic. However, the spatial extent of
these negative correlations centered on the focus regions varies across the models, and the signals of correlations outside of the
245 regions differ noticeably between some models (e.g., CESM1 and bcc-csm1-1).

In the western region (Fig. 3a), NOAH-LSM is characterized by positive correlations at high latitudes over 60°N and neg-
ative correlations at the mid-latitudes, a pattern that resembles the NAO. CESM1 and CCSM4 show to some extent the most
similar correlation patterns to NOAH-LSM. GISS-E2-R and MIROC-ESM exhibit similar positive correlations over the high
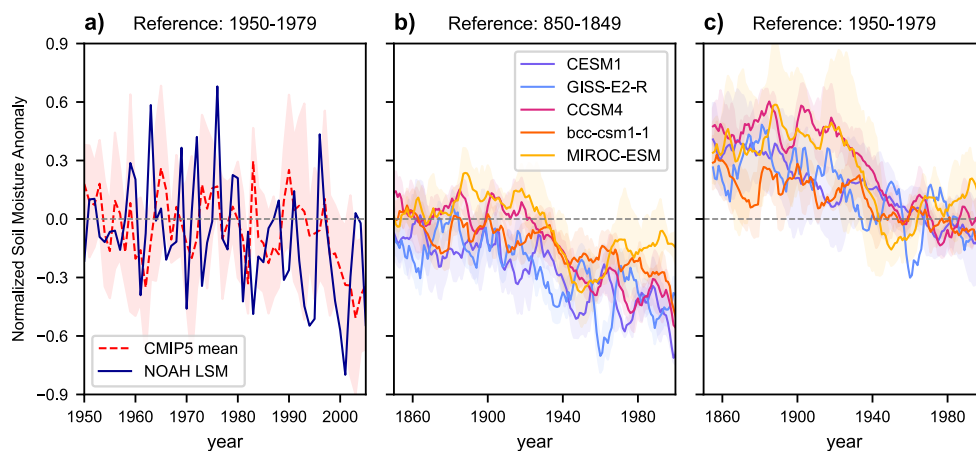
Figure 2. The annual mean time series of SOIL in the Mediterranean region (13°W–37°E, 32°–43°N) with different reference periods: (a)
from NOAH-LSM (blue line), and ensemble mean (dashed red line) and spread (shaded red; given as one standard deviation) of simulations
included in Table 1 during 1950–2005 with a reference period of 1950–1979, (b) 10-year running means (lines) and ensemble spread (shaded)
of simulations in Table 1 during 1850–2005 with a reference period of 850–1849, and (c) same as (b) but with a reference period of 1950–
1979.
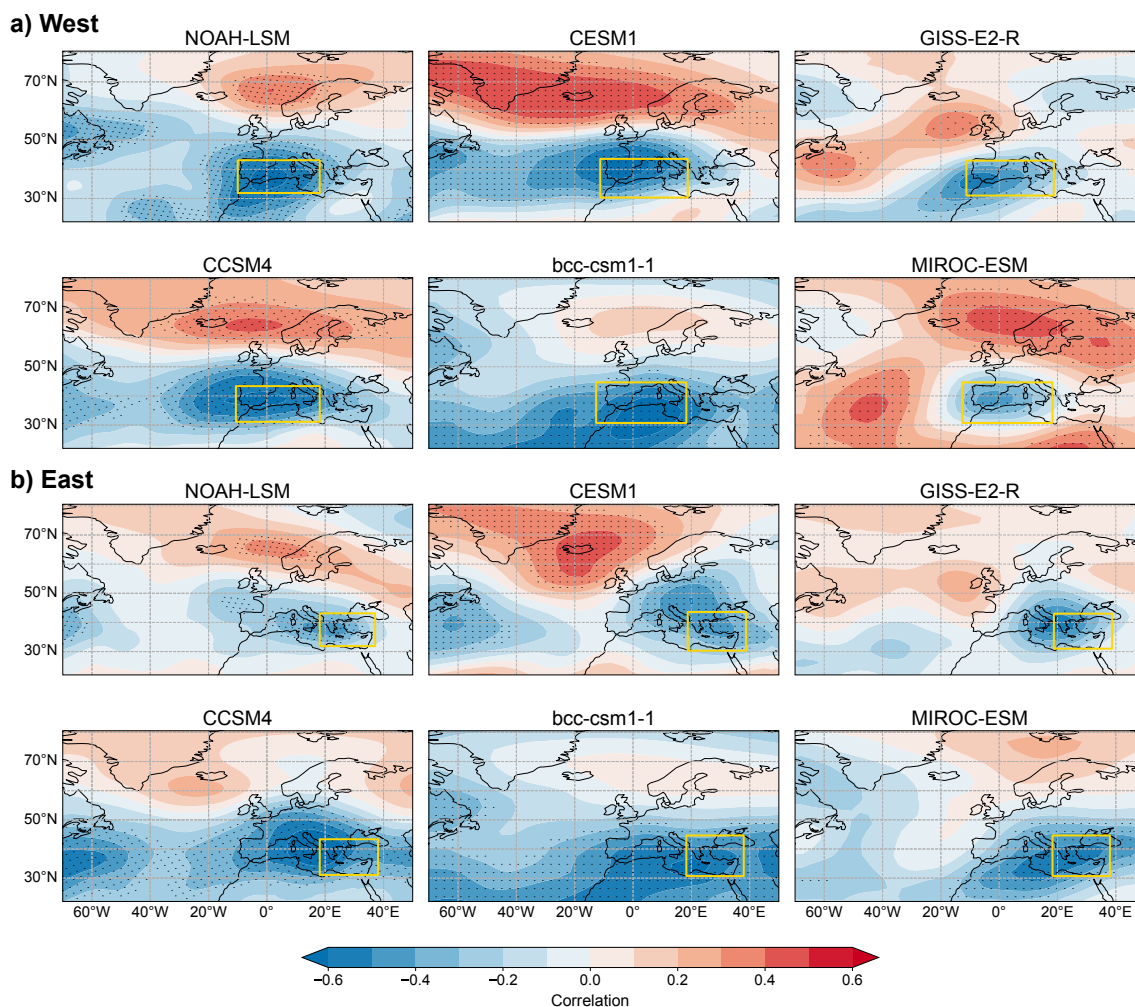
Figure 3. Pearson correlation coefficients between the time series of Z500 and SOIL in (a) the western and (b) the eastern Mediterranean. The dots highlight the regions where the correlations are statistically significant at the 5% level. Yellow squares indicate (a) the western and (b) eastern Mediterranean regions where the area-weighted soil anomalies (SOIL) are calculated. Note that the yellow squares delimiting each region differ slightly between the models since the horizontal resolutions are not interpolated to the same grid.

latitudes, but the spatial extent and location differ from those in NOAH-LSM. The bcc-csm1-1 does not present any statistically

250   significant correlations north to 50°N.

In the eastern region (Fig. 3b), NOAH-LSM shows negative correlations over southern Europe and positive correlations are found at high latitudes over the Scandinavian Peninsula. This pattern is similar to that for the western Mediterranean, but with lower values and a slightly different spatial extent. CESM1 exhibits the most similar pattern to the NOAH-LSM. The rest of the models show negative correlations over southern Europe, but the correlations outside of Europe are not significant.

255   Nevertheless, all models present similarities to the NOAH-LSM, fed with the present observational data, exhibiting a center of negative correlations in southern Europe with larger values over the focus regions. In general, CESM1 resembles the NOAH-LSM in both target regions better than the other models, although some difference exists in the spatial extent of significant correlations. The difference in correlation patterns between the models can be due to the model-dependent internal variability, and a relatively shorter time period (56 years) considered for the correlation analysis. A time series of 56 years may not include

260   all possible variability of SOIL and Z500, and could also influence the significance level of the statistical tests. A potential implication of the difference between the models on the analysis is discussed again in the coming sections.

4.2   Mediterranean drought characteristics during the last millennium (850–2005)

Before examining droughts for the entire last millennium in the climate simulations, it is necessary to recall that the drought definition is sensitive to the reference period. For instance, when 850–1849 CE (LM) is selected as the reference period to

265   calculate the soil moisture anomalies, the Mediterranean region is under a constant long-term dry condition during the entire historical period (Fig. 2b). The continuous negative SOIL in Fig. 2b indicates that the mean climate was wetter in LM than in the upcoming decades, a change that is mostly attributed to anthropogenic effects on global and regional climate (Masson-Delmotte et al., 2021). Although the magnitude of the negative trend is the same, it is noticeable that these continuous negative SOIL conditions are not apparent when the recent period (1950–1979) is considered for the anomaly calculation (Fig. 2a). To

270   analyze the entire Common Era together without the influence of the recent anthropogenic forcing, the ensemble means of SOIL are extracted from each ensemble member of Hist (Fig. 2c) as explained in Section 3.1. The time series of the number of drought years in a moving window of a century for each model and region are presented in Fig. 4. In addition, the percentage of total drought years and the mean duration of the droughts are included.

    The number of total drought years and the mean duration vary across the models. Compared to the other models, MIROC-

275   ESM shows a reduced percentage of total drought years in both regions (7.02% for the western region and 7.63% for the eastern region). The percentages of droughts in the other models range from 9.26% (GISS-E2-R) to 11.24% (CCSM4) for the west, and from 8.77% (GISS-E2-R) to 11.44% (bcc-csm1-1) for the east. The mean duration varies from 4.07 years (CCSM4) to 4.62 years (bcc-csm1-1) for the west, and 3.95 years (CESM1) to 4.71 years (MIROC-ESM) for the east. For the duration, unlike for the total drought years, MIROC-ESM shows comparable duration to other models and higher values than others in

280   the east, indicating that in MIROC-ESM there are fewer droughts but with longer duration.

    The time series of drought years (Fig. 4) show that no simultaneous period of increasing or decreasing drought events is observed between the models. For example, an apparent decrease in drought events in 1600–1650 in GISS-E2-R does not appear in any of the other models. The same happens for the no-drought period in the eastern Mediterranean during mid-1500 in CCSM4. In addition, in CESM1 and GISS-E2-R, which are the two models that have more ensemble members during LM,

285   there is large variability in drought occurrence across the ensemble members of the same model, not showing a common period with similar drought occurrence in LM. This fact emphasizes that external forcing signals do not play a role in droughts over the Mediterranean, indicating that internal variability is the primary driver of droughts in the region during LM and a counterfactual Hist without anthropogenic forcing. More precisely, although external forcing can affect drought occurrence, their influences
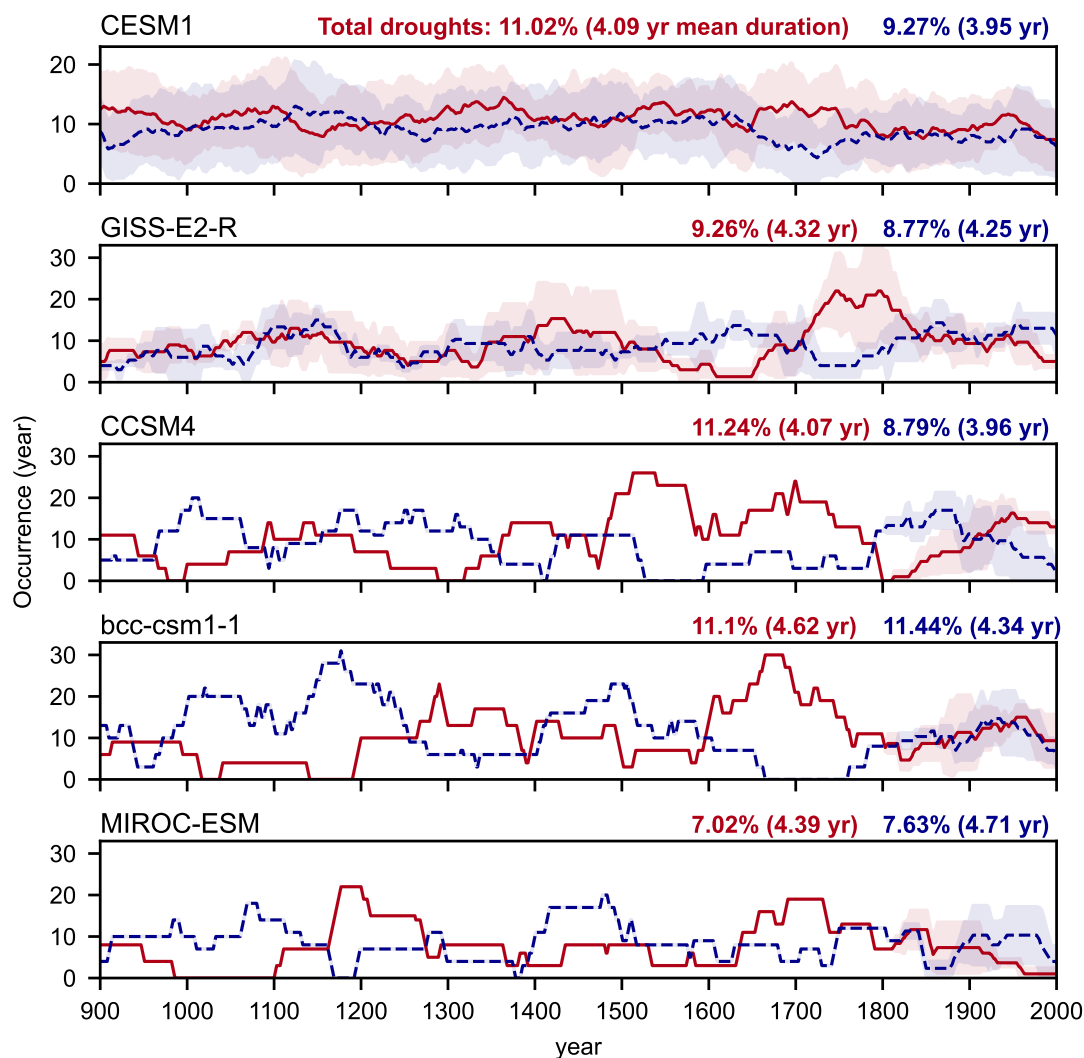
Figure 4. Occurrence of drought years in a moving window of a century in the western (red) and eastern Mediterranean (blue). The mean percentages of total drought years and mean duration of droughts appear in the top-right part of each panel. Ensemble spreads of occurrence are shaded.

are masked by internal variability. This observation is in line with previous climate model-based studies (Xoplaki et al., 2018; Kim and Raible, 2021) and proxy-based studies (Cook et al., 2016; Rao et al., 2017). Volcanic eruptions which strongly affect the global hydroclimate on a multi-year time scale are more related to wetter conditions over the Mediterranean (Iles and Hegerl, 2014; Rao et al., 2017; Kim and Raible, 2021). Although external forcing could be associated with a much longer fluctuation of dryness and wetness over the region (e.g., millennial to orbital scales; Stockhecke et al., 2016), these time scales are beyond the scope of this study.

In the simulations, an anti-phase of drought occurrence with multi-decadal time scales between the western and the eastern regions is observed, more clearly in those models and periods with one ensemble member. This anti-phase is in line with Roberts et al. (2012) and can be associated with dominant drought-driving circulation patterns of each region. More details on this are provided in the next sections. For some periods, simultaneous drought occurrence between the western and eastern regions is detected in both regions, for instance, 1100-1150 in CCSM4 and 1400-1450 in bcc-csm1-1, which seems to agree with Cook et al. (2016). However, this in-phase variability does not occur as noticeably as the anti-phase relationship in the model simulations. For those models and periods with more ensemble members, the ensemble means also exhibit this multi-decadal anti-phase relationship between the west and east, although sometimes this association is blurred by the ensemble spread. During Hist (Fig. 2b) the entire Mediterranean shows concomitant dryness reflecting the dominance of anthropogenic influence over the natural variability.

4.3 Circulation patterns associated with droughts

The PC-KCA-PCC method (Section 3.5) is used to detect drought-related circulation patterns in Z500 of the climate simulations. In total, 11 drought-associated pattern groups are detected. These pattern groups are presented in Fig. 5, with their frequencies (in the number of occurrences per century) during 850–2005. Each pattern group is a mean of a certain number of clusters. The first five pattern groups contain 83% of the entire drought years (Fig. 5). The list of models and experiments included in each pattern group are included in Table A1.

Some pattern groups resemble the well-known modes of climate variability: P1 is the combination of a high-pressure system over Europe and a positive NAO pattern. This circulation pattern is similar to those observed in the correlation composite during present day in the western Mediterranean (Fig. 3a), and it is commonly associated with Mediterranean droughts (Xoplaki et al., 2018; Kim and Raible, 2021). P2 is a negative NAO pattern with a center of negative anomalies in the mid-latitudes extending from the Atlantic Ocean to Europe. P3 is the opposite phase of P2, which resembles a positive NAO. These three patterns enclose 62% of the total occurrence, highlighting the importance of the NAO for Mediterranean droughts. P4 shows a similar high-pressure system over central and southern Europe, but with negative Z500 anomalies in the Atlantic Ocean and high latitudes. P8 seems to be the opposite phase of P4. It is a wave-train pattern extending over the northern Atlantic and Europe, resembling an EA-WR pattern. P5 is similar to the Eastern Atlantic pattern.

Besides the patterns that are comparable to the well-known modes of variability in the mid-latitudes, some patterns exhibit more unique characteristics and are derived from one model only. The spatial structure of P6 with positive Z500 in the mid-latitudes and negative Z500 in the high latitudes is similar to a positive NAO in P3, but with a distinctly different Z500 anomaly over land. This pattern only appears in GISS-E2-R. P10, characterized by positive anomalies in the Atlantic and negative anomalies in central and northern Europe, and P9 and P11, with a high-pressure system centered over the eastern Mediterranean, are all derived from MIROC-ESM.
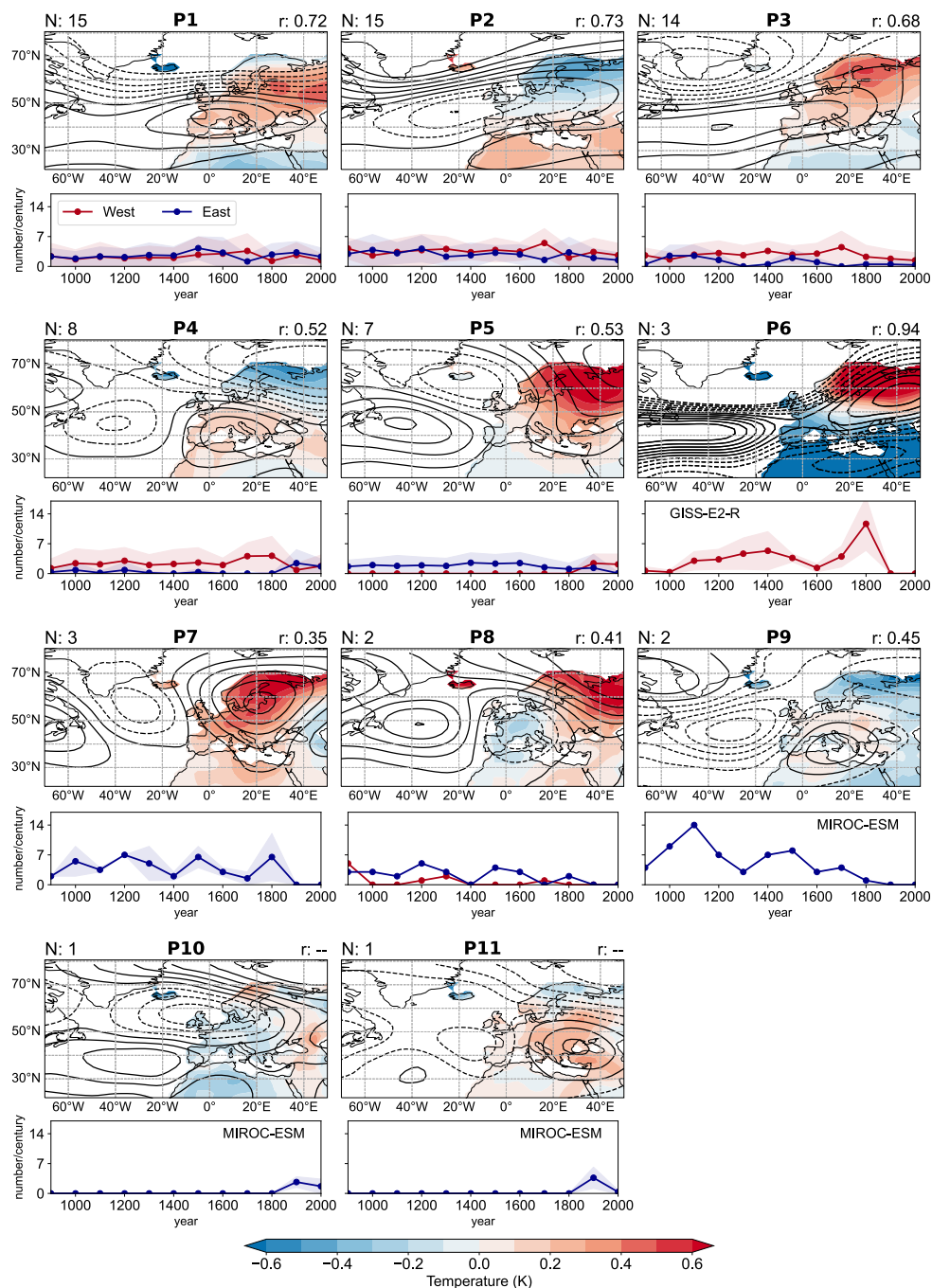
Figure 5. Extratropical pattern groups $P1$ to $P11$ associated with Mediterranean droughts, in which temperature anomalies are shaded and the contour lines show the associated Z500 field. Negative and positive Z500 values are plotted with dashed and solid lines, respectively. The number of clusters N is included on the top-left part of each map, while the mean Pearson correlation between the clusters in each pattern group r appears on the top-right part. Below each map, the time series of occurrence of droughts per century for the western (red) and eastern (blue) Mediterranean are plotted, together with the respective ensemble spread of occurrence (shaded). When only one climate model belongs to a group pattern P, its name appears on the panel. **15**

In terms of surface temperature anomalies, regions with high pressure anomalies exhibit positive temperature anomalies. Although in general, temperature conditions are not the main driver of the initiation of droughts, they can be a factor that contribute to the continuity of droughts when warm conditions occur over the target region (western or eastern Mediterranean) (Kim and Raible, 2021).

330   The frequencies of occurrence (panels below each map in Fig. 5) indicate that droughts are associated with different circulation patterns. However, some pattern groups occur more frequently than others and only in some periods. The western and eastern Mediterranean do not always share the same patterns. P1 (high-pressure system and positive NAO-like) and P2 (negative NAO-like) appear in both regions with a similar frequency over time. P3 (positive NAO-like) and P4 (high-pressure system in central and southern Europe) occur more frequently in the western region, and P6 from GISS-E2-R is only associated with

335   droughts over the western Mediterranean. P5 (EA-like) and P8 (low-pressure system in Europe) are more apparent in the east. P7 (EA-WR-like), P9 and P11 (high-pressure system in the east), and P8 are only associated with droughts over the eastern Mediterranean. Note that the last three pattern groups are from MIROC-ESM.
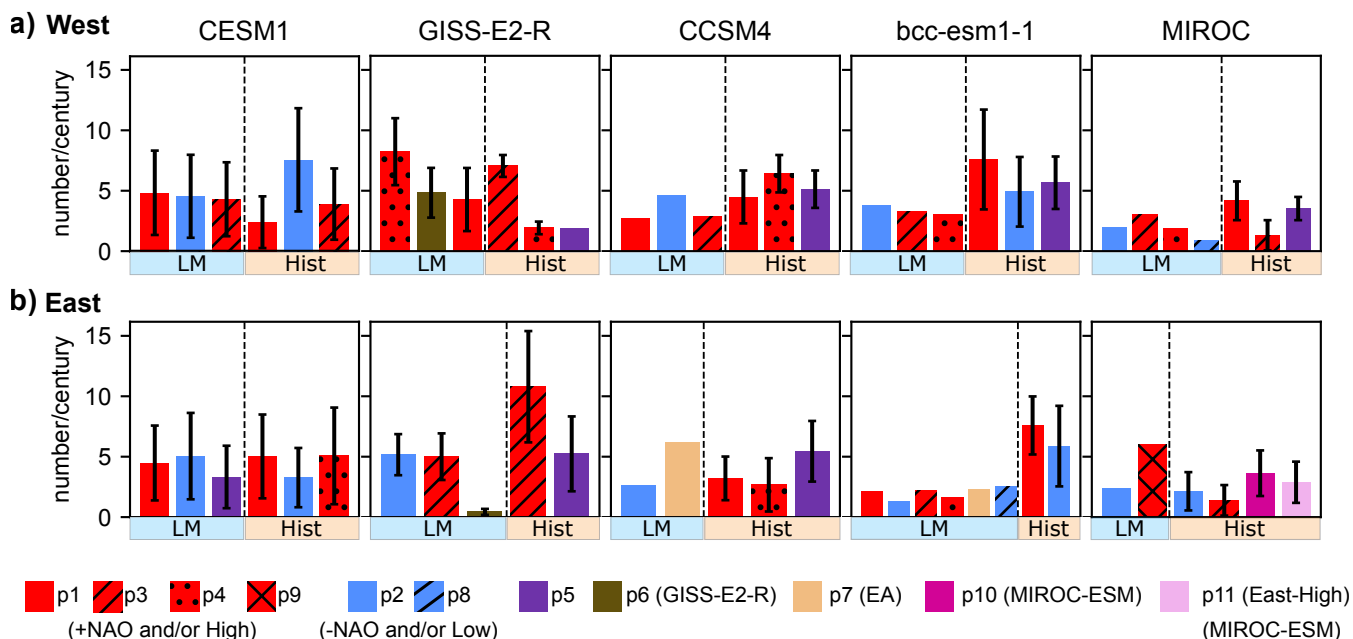
Figure 6. Mean occurrence of drought-associated pattern groups during the last millennium (LM) and historical (Hist) periods for each climate model over the (a) western and (b) eastern Mediterranean. Similar patterns in spatial Z500 anomalies are coloured with the same colour, but with different patterns. The black vertical lines indicate the spread of occurrence.

Fig. 6 shows the mean occurrence of pattern groups for each model during LM and Hist. Extended version of Fig. 6 can be found in Fig. A1 which shows the time series of occurrence of pattern groups for each climate model. For simplicity, in

340   Fig. 6, the patterns are classified by their similarity in spatial Z500 anomalies. For instance, those with high pressure over central Europe or the Atlantic Ocean and a positive NAO-like are shaded in red (positive-type pattern). The same is for the

patterns characterized by the low-pressure system and/or negative anomalies and a negative NAO-like over the same region, but in blue (negative-type pattern). Fig. 6 indicates that the positive- and negative-type patterns are shared by all models. As shown by Fig. 4, the frequencies of these patterns vary across the model and time period. In addition, some patterns are more
345 noticeable in some models than others. The EA-WR-like pattern appears in CCSM4 and bcc-csm1-1 but not in CESM1, GISS-E2-R, and MIROC-ESM. Some patterns occur dominantly during one period. For example, P6, P7, and P9 are patterns that are visible during LM. However, P10 and P11 in the eastern and P5 over the western region appear only during Hist. In addition, the ensemble spread of pattern occurrence (black bars in Fig. 6) is also an important quantity to consider as it shows large variability in the occurrence of a pattern during the same period.

350 ## 5 Discussion

It is arguable that the detected pattern groups and their frequencies depend on the numbers of N PCs and k clusters used for the method. We only take some PCs and clusters that explain an acceptable percentage of variance to increase the robustness of the clustering method. This approach may exclude certain Z500 anomalies that are outside the threshold. However, the percentage of variance in the same period is not distinctly different between the models (Table 2). They are between 72% to 78% in LM
355 (around 80% in Hist) and with $k = 3$ in most of the models (maximum 6 or 7 for a few models). Hence, it is possible that the method may be sensitive to the selected parameters and it may exclude some variability with a low occurrence, but it does not affect the comparability between the models.

Another finding is the difference in the detected patterns between LM and Hist. Some patterns appear only in one period and not in another. This difference in LM and Hist may occur because Z500 of each period are included separately in the clustering
360 method (Section 3.5), and the Hist simulations cover a much shorter period than LM. Some patterns may not occur frequently during this short period. Taking out an ensemble mean from the ensemble members may also influence the spatial patterns of Hist, as the values of ensemble means can be sensitive to the number of simulations (Maher et al., 2018). However, any statistical detrending method to exclude the recent anthropogenic forcing contains similar statistical drawbacks. For instance, the trend during Hist is not uniform over the entire period and that could cause some difficulties to select a suitable detrending
365 period in a linear or polynomial detrending method.

It needs to be pointed out that MIROC-ESM presents many unique patterns that fail to join other pattern groups, largely occurring with the eastern Mediterranean patterns. We assume that this can be related to the horizontal and vertical resolution of land grid points in MIROC-ESM. MIROC-ESM has only half of the grids compared to bcc-csm1-1 over both the western and eastern regions and presents relatively coarse vertical soil layers (Table 1). The coarse vertical and horizontal resolutions of
370 land grid points may affect the variables associated with soil moisture such as precipitation, which is sensitive to the grid size (Haren et al., 2015). Moreover, scarce land grid points and vertical levels are probably insufficient to represent land hydrology and the processes associated with precipitation (Champion et al., 2011). This can be the reason why MIROC-ESM shows correlation patterns that differs distinctly from NOAH-LSM outside the focus region (Fig. 3).

Regarding the pattern groups, in all models, NAO-like and high pressure and ridge over central Europe occur more frequently

375 in the western Mediterranean droughts. The influence of positive NAO is weaker over the eastern region, presenting a lower frequency of occurrences. The eastern region is more dominated by eastern-type patterns, such as an EA-like pattern or eastern-centered high, where the center of positive Z500 anomalies is located over the eastern Mediterranean and weak or negative Z500 anomalies are found over the western region. These findings agree with already known studies on present observation-based dry periods (Xoplaki et al., 2004, 2012). The link between the NAO and EA patterns and Mediterranean droughts is

380 also identified in a tree-ring-based reconstruction study by Cook et al. (2016) and Markonis et al. (2018). Different to the proxy-based studies, our study shows that the EA influence is largely concentrated in the eastern region.

The detected circulation patterns explain to some extent the anti-phase drought occurrence between the western and eastern Mediterranean in Fig. 4. In general, patterns involved in droughts in one region are characterized by strong positive Z500 in the focus region but by weak anomalies in another region. Such Z500 anomalies would bring dryness and warm conditions to the

385 focus region and a relatively less dry condition to another region, agreeing with Dünkeloh and Jacobeit (2003); Roberts et al. (2012). If these patterns are able to persist longer in time over a target region, that is, occurring more frequently during a certain period, then the other region may experience a long-lasting opposite condition. However, the mechanisms that maintain these interannual patterns to persist longer or to occur more frequently, contributing to a multi-decadal scale anti-phase relationship, still remain elusive. Our result showing the anti-phase drought occurrence between the west and east supports the lake sediment-

390 based reconstruction by Roberts et al. (2012) but is in contrast to the tree ring-based reconstruction by Cook et al. (2016). This difference between proxy-based reconstruction may possibly be explained by large discrepancies in different hydroclimate reconstructions and different intrinsic characteristics of each proxy (Cook et al., 2016).

Our analysis also shows that the contribution of the patterns to droughts may greatly depend on the choice of the model. For example, the importance of EA-WR in the eastern droughts is apparent in CCSM4 and bcc-csm1-1 but not in other models

395 (Fig. 6). The frequencies of a shared pattern between some models also vary greatly among them. This highlights the fact that climate models have their preferred circulation patterns associated with Mediterranean droughts.

6   Conclusions

We identify circulation patterns in the Euro-Atlantic domain associated with persistent droughts in the western and eastern Mediterranean regions during 850–2005 in several CMIP5-PMIP3 and CESM-LME climate simulations. Droughts are quanti-

400 fied through annual anomalies of vertically integrated 70 cm soil moisture and circulation patterns through the annual anomalies of geopotential height at 500 hPa.

Our findings emphasize that Mediterranean droughts are driven by internal variability, which is in line with previous studies (e.g., Cook et al., 2016; Xoplaki et al., 2018). Extratropical circulation patterns associated with Mediterranean droughts resemble the major climate patterns in the Euro-Atlantic region: western Mediterranean droughts are dominated by a high-pressure

405 system over central Europe and an NAO-like pattern, while eastern Mediterranean droughts are linked to positive pressure anomalies in the southern and eastern Mediterranean, negative NAO, EA and EA-WR like patterns. An anti-phase of drought

variability between the west and east is found in this study, which agrees with Roberts et al. (2012) and Dubrovskỳ et al. (2014). The circulation patterns also explain the anti-phase behaviour in the western versus the eastern Mediterranean. However, the mechanisms that drive the persistence of these patterns leading to a multi-decadal scale relationship remain elusive. This anti-phase variability is not apparent when the GHG-forced signal is included from 1850. In this case, both the western and eastern Mediterranean show a coherent decrease in soil moisture anomalies.

Some circulation patterns associated with droughts occur more frequently than others, but not a single pattern dominates a certain region and period. Some patterns are only apparent in one model, indicating that the main drivers of droughts are different between the models. Moreover, large discrepancies in drought occurrence exist between the models and within the ensemble members of the models. This observation highlights model-dependent internal variability. Model differences in drought occurrence and patterns can be also attributed to the resolution of a model: coarse horizontal and vertical resolutions of land grid points may not reflect well the soil moisture variability and its associated circulation. All these differences between the models can be a source of uncertainty that complicates model-proxy comparisons.

This work attempts to identify drought-associated extratropical circulations, focusing on natural climate variability, in each individual climate model. In this way, differences between the models are identified better including how they represent the baseline climate for droughts. Our results can be helpful in understanding model discrepancies and uncertainties in future drought projections, for instance, to examine which drought-associated modes of climate variability are preferred by each model, and how these modes will change under different climate change conditions. A more detailed understanding of these differences may contribute to better future projections, hence, aid long-term preparedness for droughts over the region.

Code and data availability. The codes to reproduce the analysis performed in this manuscript will be available on GitHub upon acceptance of the manuscript. All the datasets used in this study are freely available online: CMIP5 at https://esgf-node.llnl.gov/projects/cmip5/, ERA5 at https://cds.climate.copernicus.eu/, and NOAH-LSM soil moisture at https://disc.gsfc.nasa.gov/datasets/GLDAS_NOAH025_3H_2.1/summary.

Author contributions. WMK designed the study and conducted the analysis in discussion with CCR. WMK set up the methodology with the input of SJGR. WMK and SJGR prepared the first draft of the manuscript. All authors contributed to the scientific discussion and writing of the manuscript.

Competing interests. The authors declare that they have no conflict of interest.

Acknowledgements. We acknowledge the World Climate Research Programme's Working Group on Coupled Modelling, which is responsible for CMIP, and we thank the climate modeling groups (listed in Table 1 of this paper) for producing and making available their model

435   output. For CMIP the U.S. Department of Energy's Program for Climate Model Diagnosis and Intercomparison provides coordinating support and led development of software infrastructure in partnership with the Global Organization for Earth System Science Portals. We also acknowledge the Copernicus program for the ERA5 data (Hersbach et al., 2018) available in Copernicus Climate Change Service Climate Data Store, and the NASA/NOAA Global Land Data Assimilation System for the Noah Land Surface Model dataset (Rodell et al., 2004). WMK acknowledge funding from the Swiss National Science Foundation (SNF; grant number P500PN_206653). CCR is supported by the
440   SNF (grant numbers 200020_172745 and 200020_200492) and Swiss National Supercomputing Centre (CSCS).

Appendix A: Appendix

Table A1. Models and experiments pertaining to each pattern group after applying the PC-KCA-PCC method.

	West	East
p1	CESM1-LM, CESM1-H, GISS-E2-R-H, CCSM4-LM, CCSM4-H, bcc-csm1-1-H, MIROC-ESM-H	CESM1-LM, CESM1-H, CCSM4-H, bcc-csm1-1-LM, bcc-csm1-1-H
p2	CESM1-LM, CESM1-H, CCSM4-LM, bcc-csm1-1-LM, bcc-csm1-1-H, MIROC-ESM-LM	CESM1-LM, CESM1-H, GISS-E2-R-LM, CCSM4-LM, bcc-csm1-1-LM, bcc-csm1-1-H, MIROC-ESM-LM, MIROC-ESM-H
p3	CESM1-LM, CESM1-H, GISS-E2-R-H, CCSM4-LM, bcc-csm1-1-LM, MIROC-ESM-LM, MIROC-ESM-H	GISS-E2-R-LM, GISS-E2-R-H, bcc-csm1-1-LM, GISS-E2-R-H, MIROC-ESM-H,
p4	GISS-E2-R-LM, GISS-E2-R-H, CCSM4-H, bcc-csm1-1-LM, MIROC-ESM-LM	CESM1-H, CCSM4-H, bcc-csm1-1-LM
p5	GISS-E2-R-H, bcc-csm1-1-H, CCSM4-H, MIROC-ESM-H	CESM1-LM, CCSM4-H, GISS-E2-R-H
p6	GISS-E2-R-LM	
p7		CCSM4-LM, bcc-csm1-1-LM
p8	MIROC-ESM-LM	bcc-csm1-1-LM
p9		MIROC-ESM-LM
p10		MIROC-ESM-H
p11		MIROC-ESM-H
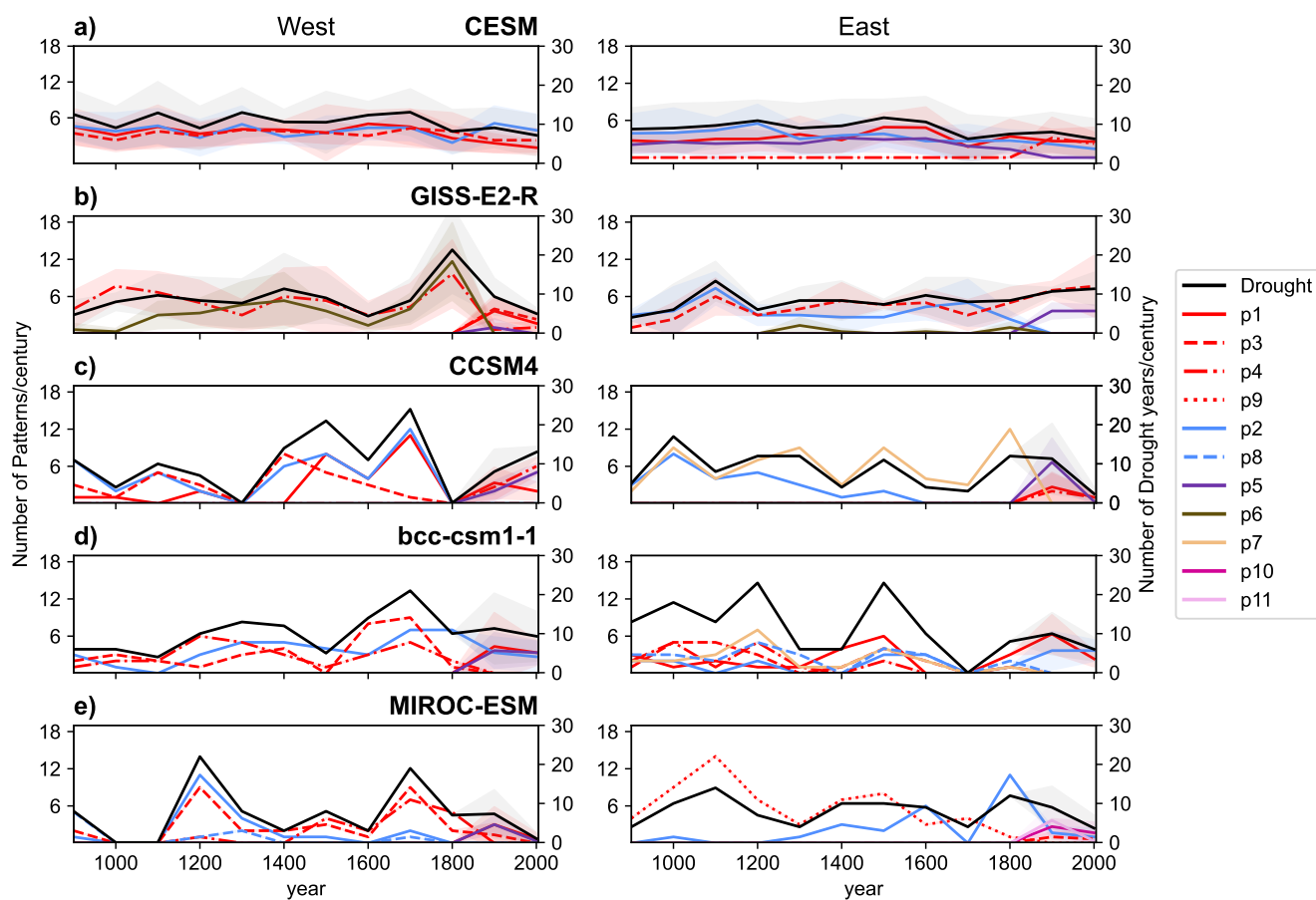
Figure A1. Extended version of Fig. 6: occurrence of each pattern group every century for each climate model.

References

Baek, S. H., Smerdon, J. E., Coats, S., Williams, A. P., Cook, B. I., Cook, E. R., and Seager, R.: Precipitation, Temperature, and Teleconnection Signals across the Combined North American, Monsoon Asia, and Old World Drought Atlases, Journal of Climate, 30, 7141–7155, https://doi.org/10.1175/JCLI-D-16-0766.1, publisher: American Meteorological Society Section: Journal of Climate, 2017.

445

Champion, A. J., Hodges, K. I., Bengtsson, L. O., Keenlyside, N. S., and Esch, M.: Impact of increasing resolution and a warmer climate on extreme weather from Northern Hemisphere extratropical cyclones, Tellus A: Dynamic meteorology and oceanography, 63, 893–906, https://doi.org/10.1111/j.1600-0870.2011.00538.x, 2011.

Coats, S., Smerdon, J. E., Seager, R., Cook, B. I., and González-Rouco, J. F.: Megadroughts in southwestern North America in ECHO-G millennial simulations and their comparison to proxy drought reconstructions, Journal of climate, 26, 7635–7649, https://doi.org/10.1175/JCLI-D-12-00603.1, 2013.

450

Cook, B. I., Anchukaitis, K. J., Touchan, R., Meko, D. M., and Cook, E. R.: Spatiotemporal drought variability in the Mediterranean over the last 900 years, Journal of Geophysical Research: Atmospheres, 121, 2060–2074, https://doi.org/10.1002/2015JD023929, 2016.

Cook, E. R., Seager, R., Kushnir, Y., Briffa, K. R., Büntgen, U., Frank, D., Krusic, P. J., Tegel, W., Schrier, G. v. d., Andreu-Hayles, L., Baillie, M., Baittinger, C., Bleicher, N., Bonde, N., Brown, D., Carrer, M., Cooper, R., Čufar, K., Dittmar, C., Esper, J., Griggs, C., Gunnarson, B., Günther, B., Gutierrez, E., Haneca, K., Helama, S., Herzig, F., Heussner, K.-U., Hofmann, J., Janda, P., Kontic, R., Köse, N., Kyncl, T., Levanič, T., Linderholm, H., Manning, S., Melvin, T. M., Miles, D., Neuwirth, B., Nicolussi, K., Nola, P., Panayotov, M., Popa, I., Rothe, A., Seftigen, K., Seim, A., Svarva, H., Svoboda, M., Thun, T., Timonen, M., Touchan, R., Trotsiuk, V., Trouet, V., Walder, F., Ważny, T., Wilson, R., and Zang, C.: Old World megadroughts and pluvials during the Common Era, Science Advances, 1, e1500 561,

455

460
https://doi.org/10.1126/sciadv.1500561, 2015.

Cos, J., Doblas-Reyes, F., Jury, M., Marcos, R., Bretonnière, P.-A., and Samsó, M.: The Mediterranean climate change hotspot in the CMIP5 and CMIP6 projections, Earth System Dynamics, 13, 321–340, https://doi.org/10.5194/esd-13-321-2022, publisher: Copernicus GmbH, 2022.

Dirmeyer, P. A.: The terrestrial segment of soil moisture–climate coupling, Geophysical Research Letters, 38, https://doi.org/10.1029/2011GL048268, _eprint: https://onlinelibrary.wiley.com/doi/pdf/10.1029/2011GL048268, 2011.

465

Dubrovskỳ, M., Hayes, M., Duce, P., Trnka, M., Svoboda, M., and Zara, P.: Multi-GCM projections of future drought and climate variability indicators for the Mediterranean region, Regional Environmental Change, 14, 1907–1919, https://doi.org/10.1007/s10113-013-0562-z, 2014.

Dünkeloh, A. and Jacobeit, J.: Circulation dynamics of Mediterranean precipitation variability 1948–98, International Journal of Climatology: A Journal of the Royal Meteorological Society, 23, 1843–1866, https://doi.org/10.1002/joc.973, 2003.

470

Esit, M., Kumar, S., Pandey, A., Lawrence, D. M., Rangwala, I., and Yeager, S.: Seasonal to multi-year soil moisture drought forecasting, npj Climate and Atmospheric Science, 4, 1–8, https://doi.org/10.1038/s41612-021-00172-z, number: 1 Publisher: Nature Publishing Group, 2021.

Gao, Y. and Gao, C.: European hydroclimate response to volcanic eruptions over the past nine centuries, International Journal of Climatology, 37, 4146–4157, https://doi.org/10.1002/joc.5054, 2017.

475

Ghannam, K., Nakai, T., Paschalis, A., Oishi, C. A., Kotani, A., Igarashi, Y., Kumagai, T., and Katul, G. G.: Persistence and memory timescales in root-zone soil moisture dynamics, Water Resources Research, 52, 1427–1445, https://doi.org/10.1002/2015WR017983, 2016.

Hannachi, A., Jolliffe, I. T., and Stephenson, D. B.: Empirical orthogonal functions and related techniques in atmospheric science: A review,
480   International Journal of Climatology, 27, 1119–1152, https://doi.org/https://doi.org/10.1002/joc.1499, 2007.

Haren, R. v., Haarsma, R. J., Oldenborgh, G. J. V., and Hazeleger, W.: Resolution Dependence of European Precipitation in a State-of-the-
       Art Atmospheric General Circulation Model, Journal of Climate, 28, 5134–5149, https://doi.org/10.1175/JCLI-D-14-00279.1, publisher:
       American Meteorological Society Section: Journal of Climate, 2015.

Hersbach, H., Bell, B., Berrisford, P., Biavati, G., Horányi, A., Muñoz Sabater, J., Nicolas, J., Peubey, C., Radu, R., Rozum, I., et al.: ERA5
485   hourly data on single levels from 1979 to present, (Accessed on December 28, 2021), 10.24381/cds.adbb2d47, 2018.

Hersbach, H., Bell, B., Berrisford, P., Hirahara, S., Horányi, A., Muñoz-Sabater, J., Nicolas, J., Peubey, C., Radu, R., Schepers, D., Sim-
       mons, A., Soci, C., Abdalla, S., Abellan, X., Balsamo, G., Bechtold, P., Biavati, G., Bidlot, J., Bonavita, M., Chiara, G. D., Dahlgren,
       P., Dee, D., Diamantakis, M., Dragani, R., Flemming, J., Forbes, R., Fuentes, M., Geer, A., Haimberger, L., Healy, S., Hogan, R. J.,
       Hólm, E., Janisková, M., Keeley, S., Laloyaux, P., Lopez, P., Lupu, C., Radnoti, G., Rosnay, P. d., Rozum, I., Vamborg, F., Vil-
490   laume, S., and Thépaut, J.-N.: The ERA5 global reanalysis, Quarterly Journal of the Royal Meteorological Society, 146, 1999–2049,
       https://doi.org/https://doi.org/10.1002/qj.3803, _eprint: https://rmets.onlinelibrary.wiley.com/doi/pdf/10.1002/qj.3803, 2020.

Iles, C. E. and Hegerl, G. C.: The global precipitation response to volcanic eruptions in the CMIP5 models, Environmental Research Letters,
       9, 104 012, https://doi.org/10.1088/1748-9326/9/10/104012, publisher: IOP Publishing, 2014.

Kim, W. M. and Raible, C. C.: Dynamics of the Mediterranean droughts from 850 to 2099 CE in the Community Earth System Model,
495   Climate of the Past, 17, 887–911, https://doi.org/10.5194/cp-17-887-2021, publisher: Copernicus GmbH, 2021.

Kopparla, P., Fischer, E. M., Hannay, C., and Knutti, R.: Improved simulation of extreme precipitation in a high-resolution atmosphere model,
       Geophysical Research Letters, 40, 5803–5808, https://doi.org/10.1002/2013GL057866, 2013.

Krichak, S. O. and Alpert, P.: Decadal trends in the east Atlantic–west Russia pattern and Mediterranean precipitation, International journal
       of climatology: a journal of the Royal Meteorological Society, 25, 183–192, https://doi.org/10.1002/joc.1124, 2005.

500   Lehner, F., Joos, F., Raible, C. C., Mignot, J., Born, A., Keller, K. M., and Stocker, T. F.: Climate and carbon cycle dynamics in a CESM
       simulation from 850 to 2100 CE, Earth System Dynamics, 6, 411–434, https://doi.org/10.5194/esd-6-411-2015, publisher: Copernicus
       GmbH, 2015.

Lehner, F., Coats, S., Stocker, T. F., Pendergrass, A. G., Sanderson, B. M., Raible, C. C., and Smerdon, J. E.: Projected drought risk in 1.5 C
       and 2 C warmer climates, Geophysical Research Letters, 44, 7419–7428, https://doi.org/10.1002/2017GL074117, 2017.

505   Lionello, P., Malanotte-Rizzoli, P., and Boscolo, R.: Mediterranean Climate Variability, Elsevier, 2006.

Maher, N., Matei, D., Milinski, S., and Marotzke, J.: ENSO change in climate projections: forced response or internal variability?, Geophys-
       ical Research Letters, 45, 11–390, https://doi.org/10.1029/2018GL079764, 2018.

Markonis, Y., Hanel, M., Máca, P., Kyselý, J., and Cook, E. R.: Persistent multi-scale fluctuations shift European hydroclimate to its millen-
       nial boundaries, Nature Communications, 9, 1767, https://doi.org/10.1038/s41467-018-04207-7, number: 1 Publisher: Nature Publishing
510   Group, 2018.

Masson-Delmotte, V., Zhai, P., Pirani, A., Connors, S. L., Péan, C., Berger, S., Caud, N., Chen, Y., Goldfarb, L., Gomis, M., et al.: Climate
       change 2021: the physical science basis, Contribution of working group I to the sixth assessment report of the intergovernmental panel on
       climate change, 2, 1513–1766, https://doi.org/:10.1017/9781009157896.013, 2021.

Monahan, A. H., Fyfe, J. C., Ambaum, M. H. P., Stephenson, D. B., and North, G. R.: Empirical Orthogonal Functions: The Medium is the
515   Message, Journal of Climate, 22, 6501 – 6514, https://doi.org/10.1175/2009JCLI3062.1, 2009.

Otto-Bliesner, B. L., Brady, E. C., Fasullo, J., Jahn, A., Landrum, L., Stevenson, S., Rosenbloom, N., Mai, A., and Strand, G.: Climate Variability and Change since 850 CE: An Ensemble Approach with the Community Earth System Model, Bulletin of the American Meteorological Society, 97, 735–754, https://doi.org/10.1175/BAMS-D-14-00233.1, publisher: American Meteorological Society Section: Bulletin of the American Meteorological Society, 2016.

520 PAGES Hydro2k Consortium et al.: Comparing proxy and model estimates of hydroclimate variability and change over the Common Era, Climate of the Past, 13, 1851–1900, 2017.

Previdi, M. and Liepert, B. G.: Annular modes and Hadley cell expansion under global warming, Geophysical Research Letters, 34, https://doi.org/10.1029/2007GL031243, 2007.

Rao, M. P., Cook, B. I., Cook, E. R., D'Arrigo, R. D., Krusic, P. J., Anchukaitis, K. J., LeGrande, A. N., Buckley, B. M., Davi, N. K.,
525 Leland, C., and Griffin, K. L.: European and Mediterranean hydroclimate responses to tropical volcanic forcing over the last millennium, Geophysical Research Letters, 44, 5104–5112, https://doi.org/10.1002/2017GL073057, 2017.

Roberts, N., Moreno, A., Valero-Garcés, B. L., Corella, J. P., Jones, M., Allcock, S., Woodbridge, J., Morellón, M., Luterbacher, J., Xoplaki, E., et al.: Palaeolimnological evidence for an east–west climate see-saw in the Mediterranean since AD 900, Global and Planetary Change, 84, 23–34, https://doi.org/10.1016/j.gloplacha.2011.11.002, 2012.

530 Rodell, M., Houser, P., Jambor, U., Gottschalck, J., Mitchell, K., Meng, C.-J., Arsenault, K., Cosgrove, B., Radakovich, J., Bosilovich, M., et al.: The global land data assimilation system, Bulletin of the American Meteorological society, 85, 381–394, https://doi.org/10.1175/BAMS-85-3-381, 2004.

Rodwell, M. J. and Hoskins, B. J.: Monsoons and the dynamics of deserts, Quarterly Journal of the Royal Meteorological Society, 122, 1385–1404, https://doi.org/10.1002/qj.49712253408, 1996.

535 Samaniego, L., Thober, S., Kumar, R., Wanders, N., Rakovec, O., Pan, M., Zink, M., Sheffield, J., Wood, E. F., and Marx, A.: Anthropogenic warming exacerbates European soil moisture droughts, Nature Climate Change, 8, 421–426, https://doi.org/10.1038/s41558-018-0138-5, 2018.

Schmidt, G. A., Jungclaus, J. H., Ammann, C. M., Bard, E., Braconnot, P., Crowley, T. J., Delaygue, G., Joos, F., Krivova, N. A., Muscheler, R., Otto-Bliesner, B. L., Pongratz, J., Shindell, D. T., Solanki, S. K., Steinhilber, F., and Vieira, L. E. A.: Climate forc-
540 ing reconstructions for use in PMIP simulations of the Last Millennium (v1.1), Geoscientific Model Development, pp. 185–191, https://doi.org/https://doi.org/10.5194/gmd-5-185-2012, 2012.

Shahapure, K. R. and Nicholas, C.: Cluster quality analysis using silhouette score, in: 2020 IEEE 7th International Conference on Data Science and Advanced Analytics (DSAA), pp. 747–748, IEEE, https://ieeexplore.ieee.org/document/9260048, 2020.

Spinoni, J., Barbosa, P., Bucchignani, E., Cassano, J., Cavazos, T., Christensen, J. H., Christensen, O. B., Coppola, E., Evans, J., Geyer,
545 B., et al.: Future global meteorological drought hot spots: a study based on CORDEX data, Journal of Climate, 33, 3635–3661, https://doi.org/10.1175/JCLI-D-19-0084.1, 2020.

Stevenson, S., Fasullo, J. T., Otto-Bliesner, B. L., Tomas, R. A., and Gao, C.: Role of eruption season in reconciling model and proxy responses to tropical volcanism, Proceedings of the National Academy of Sciences, 114, 1822–1826, https://doi.org/10.1073/pnas.1612505114, publisher: Proceedings of the National Academy of Sciences, 2017.

550 Stockhecke, M., Timmermann, A., Kipfer, R., Haug, G. H., Kwiecien, O., Friedrich, T., Menviel, L., Litt, T., Pickarski, N., and Anselmetti, F. S.: Millennial to orbital-scale variations of drought intensity in the Eastern Mediterranean, Quaternary Science Reviews, 133, 77–95, https://doi.org/10.1016/j.quascirev.2015.12.016, 2016.

Taylor, K. E., Stouffer, R. J., and Meehl, G. A.: An Overview of CMIP5 and the Experiment Design, Bulletin of the American Meteorological Society, 93, 485–498, https://doi.org/10.1175/BAMS-D-11-00094.1, 2012.

555 Tramblay, Y., Koutroulis, A., Samaniego, L., Vicente-Serrano, S. M., Volaire, F., Boone, A., Le Page, M., Llasat, M. C., Albergel, C., Burak, S., Cailleret, M., Kalin, K. C., Davi, H., Dupuy, J.-L., Greve, P., Grillakis, M., Hanich, L., Jarlan, L., Martin-StPaul, N., Martínez-Vilalta, J., Mouillot, F., Pulido-Velazquez, D., Quintana-Seguí, P., Renard, D., Turco, M., Türkeş, M., Trigo, R., Vidal, J.-P., Vilagrosa, A., Zribi, M., and Polcher, J.: Challenges for drought assessment in the Mediterranean region under future climate scenarios, Earth-Science Reviews, 210, 103 348, https://doi.org/10.1016/j.earscirev.2020.103348, 2020.

560 Tuel, A. and Eltahir, E. A.: Why is the Mediterranean a climate change hot spot?, Journal of Climate, 33, 5829–5843, https://doi.org/10.1175/JCLI-D-19-0910.1, 2020.

Wilks, D. S.: Statistical methods in the atmospheric sciences, vol. 100, Academic press, 2011.

Wu, Y., Ting, M., Seager, R., Huang, H.-P., and Cane, M. A.: Changes in storm tracks and energy transports in a warmer climate simulated by the GFDL CM2. 1 model, Climate dynamics, 37, 53–72, https://doi.org/10.1007/s00382-010-0776-4, 2011.

565 Xoplaki, E., González-Rouco, J., Luterbacher, J., and Wanner, H.: Wet season Mediterranean precipitation variability: influence of large-scale dynamics and trends, Climate dynamics, 23, 63–78, 2004.

Xoplaki, E., Trigo, R., García-Herrera, R., Barriopedro, D., D'andrea, F., Fischer, E., Gimeno, L., Gouveia, C., Hernández, E., Kuglitsch, F., et al.: Large-scale atmospheric circulation driving extreme climate events in the Mediterranean and related impacts (chapitre 6), https://doi.org/10.1016/B978-0-12-416042-2.00006-9, 2012.

570 Xoplaki, E., Luterbacher, J., Wagner, S., Zorita, E., Fleitmann, D., Preiser-Kapeller, J., Sargent, A. M., White, S., Toreti, A., Haldon, J. F., Mordechai, L., Bozkurt, D., Akçer-Ön, S., and Izdebski, A.: Modelling Climate and Societal Resilience in the Eastern Mediterranean in the Last Millennium, Human Ecology, 46, 363–379, https://doi.org/10.1007/s10745-018-9995-9, 2018.

Yin, J. H.: A consistent poleward shift of the storm tracks in simulations of 21st century climate, Geophysical Research Letters, 32, https://doi.org/10.1029/2005GL023684, 2005.

575 Zhou, S., Williams, A. P., Berg, A. M., Cook, B. I., Zhang, Y., Hagemann, S., Lorenz, R., Seneviratne, S. I., and Gentine, P.: Land–atmosphere feedbacks exacerbate concurrent soil drought and atmospheric aridity, Proceedings of the National Academy of Sciences, 116, 18 848–18 853, https://doi.org/10.1073/pnas.1904955116, publisher: National Academy of Sciences Section: Physical Sciences, 2019.

Zscheischler, J., Mahecha, M. D., and Harmeling, S.: Climate classifications: the value of unsupervised clustering, Procedia Computer Science, 9, 897–906, https://doi.org/10.1016/j.procs.2012.04.096, 2012.